Dalton Transactions

Accepted Manuscript

ROYAL SOCIETY OF CHEMISTRY

www.rsc.org/dalton

Journal Name

ARTICLE

CO_2 Adsorption of Three Isostructural Metal-Organic Frameworks Depending on the Incorporated Highly Polarized Heterocyclic Moieties

Received 00th January 20xx,
Accepted 00th January 20xx

DOI: 10.1039/x0xx00000x

www.rsc.org/

Chengling Song,[a] Yajing Ling,[a] Liting Jin,[a] Mingxing Zhang,[b] De-Li Chen,[c*] and Yabing He[a*]

A systematical investigation of CO_2 adsorption behavior in three metal-organic frameworks was executed. The three MOFs adopted the same NbO-type structure, except that the organic ligands were grafted with different highly polarized heterocyclic moieties, namely, oxadiazole, thiadiazole, and selenadiazole, respectively. After activation, the three MOF materials showed different surface areas and pore volumes depending on the incorporated heterocyclic rings attached to the organic ligands as well as the MOF's stabilities. Among the three MOF materials, **ZJNU-41a** exhibited impressive CO_2 uptake capacity of 97.4 cm^3 (STP) g^{-1} at 298 K and 1 atm, which is comparable and even superior to those reported in NbO-type MOFs. In particular, when the molecular dipole of the attached heterocyclic moieties increases, the CO_2 uptake also increases, which was further supported by comprehensive quantum chemical calculations. This work demonstrates that the introduction of highly polarized heterocyclic functional groups into frameworks is a promising approach to target porous metal-organic framework materials with improved CO_2 adsorption performance.

1. Introduction

Metal-organic frameworks (MOFs)[1], also known as porous coordination polymers (PCPs)[2], are a rapidly expanding class of porous crystalline materials constructed by self-assembly of metal-containing clusters (typically termed as secondary building units (SBUs)) and multitopic bridging organic linkers *via* metal coordination bonds. Due to their particular and favourable structure features such as high surface area, uniform but tuneable pore size and chemically modifiable pore surface, MOFs were actively investigated in the past decades for their potential applications including gas storage/separation,[3] heterogeneous catalysis,[4] molecule sensing,[5] drug delivery,[6] etc.

Among numerous MOFs, a fascinating NbO-type of MOFs constructed from square planar dicopper paddlewheel SBUs and 4-connected diisophthalate linkers have gained extensive attention due to their unique structures featuring open metal sites and two different types of nanocages suitable for gas adsorption.[7] More significantly, when different functional groups are grafted into diisophthalate organic linkers, the corresponding frameworks, in most cases, still adopt the same NbO-type structure, thus providing an ideal platform to investigate the effect of the functional groups on gas adsorption. In fact, various diisophthalate organic linkers attached with different organic functional groups have been synthesized and employed to construct such versatile NbO-type MOF materials.[8] For example, a series of NbO-type MOFs have been reported by Schröder and co-workers studying the impact of pore size, ligand functionalization and exposed metal sites on H_2 adsorption.[8i]

To enhance CO_2 adsorption of NbO-type MOFs, great efforts are devoted to enhancing the CO_2 binding affinity toward the MOFs. Due to the inherent acidity and polarity of CO_2 molecules, one commonly employed method is adding Lewis basic or polar functional groups into the organic linkers to increase CO_2-framework interactions, with its own advantages such as very wide chemical diversity of possible functional groups. For example, Zheng *et al.* demonstrated that an amide modified porous NbO-type MOF displayed high CO_2 uptake capacity of 156.4 cm^3 (STP) g^{-1} at 273 K and 1 bar, which is attributed to favourable interactions between the CO_2 molecules and the amide groups of MOF.[9] Zhang *et al.* reported a polar NO_2-decorated NbO-type MOF exhibiting much higher CO_2 uptakes than the parent MOF NOTT-101.[8c] Recently, we also used a diisophthalate H_4L2 shown in Scheme 1, which was functionalized with highly polarized thiadiazole heterocyclic moieties, for synthesizing NbO-type **ZJNU-40** exhibiting high capacities for selective CO_2 uptake.[10] According to our reported results, it is envisaged that heterocyclic subunits with similar structure but different polarizability

[a] College of Chemistry and Life Sciences, Zhejiang Normal University, Jinhua 321004, China. E-mail: heyabing@zjnu.cn
[b] State Key Laboratory of Coordination Chemistry, School of Chemistry and Chemical Engineering, Nanjing University, Nanjing 210093, China.
[c] Key Laboratory of the Ministry of Education for Advanced Catalysis Materials, Institute of Physical Chemistry, Zhejiang Normal University. E-mail: chendl@zjnu.cn

† Footnotes relating to the title and/or authors should appear here.
Electronic Supplementary Information (ESI) available: PXRD (Fig. S1); TGA (Fig. S2); BET and Langmuir plots (Fig. S3-5); CO_2 adsorption isotherms (Fig. S6-8); PSD (Fig. S9); NMR (Fig. S10); NMR (Fig. S11-13); Crystal data and structure refinement parameters (Table S1), CCDC 1413736-1413737. See DOI: 10.1039/x0xx00000x

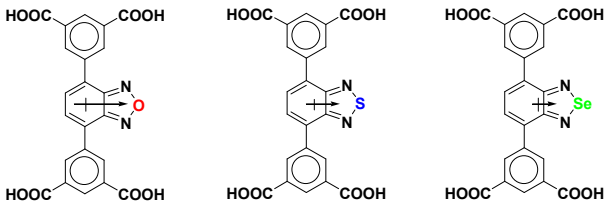

Scheme 1 The organic linkers used to synthesize **ZJNU-41**, **ZJNU-40** and **ZJNU-42**. For each linker, the dipole moment (μ) calculated using chem3D software is given below the molecular structure.

could be used to finely tune the binding interaction between CO_2 and frameworks and thus to adjust CO_2 uptakes. To extend this work, we have designed and synthesized two more new diisophthalate organic linkers H_4L1 and H_4L3, shown in Scheme 1, to which two heterocyclic units with similar structure but different polarizability were attached, namely, oxadiazole, and selenadiazole, which are very common polar groups encountered in light emitting materials, and targeted the corresponding NbO-type MOFs. Herein we wish to report on the successful preparation, structural characterization as well as CO_2 adsorption properties of three isostructural MOFs constructed from these new designed organic ligands, with the aim to systematically investigate the impact of polarized heterocyclic rings on CO_2 adsorption.

2. Experimental

2.1 Materials and measurements

All reagents and solvents were purchased from commercial sources and used as received without further purification unless otherwise specified. The dibromo intermediates used to synthesize the organic linkers, 4,7-dibromobenzo[c][1,2,5]oxadiazole,[11] and 4,7-dibromobenzo[c][1,2,5]selenadiazole,[12] were prepared according to literature methods. ^{1}H and ^{13}C NMR spectra were recorded at a Bruke Avance 600 or 400 spectrometer at room temperature. Infrared spectra (FTIR) were recorded in the 4000-400 cm^{-1} region on a FTIR spectrometer using KBr pellets. Elemental analyses (C, H and N) were performed using a Perkin–Elmer 240 CHN analysers. Thermogravimetric analysis (TGA) was performed under a flowing nitrogen atmosphere with a Netzsch STA 449C thermal analyser at a heating rate of 5 K min^{-1} in the temperature range from room temperature to 1073 K. The powder X-ray diffraction measurement was recorded on a Philips PW3040/60 automated powder diffractometer using Cu-K_α radiation (λ = 1.542 Å). Low-pressure gas adsorption isotherms were investigated with a Micrometrics ASAP 2020 HD88 surface area and porosity analyser system using the extra-high pure gases. The gases used had the following specifications (volume percentage): N_2 99.9999%, and CO_2 99.999%.

2.2 X-ray crystallography

Diffraction measurements for the MOFs, **ZJNU-41**, and **ZJNU-42**, were carried out using a Bruker APEX II diffractometer equipped with a graphite-monochromatized Mo-K_α radiation at 100(2) K. The crystal structures were solved by direct methods using the programs SHELXS-97.[13] All non-hydrogen atoms were refined anisotropically by full matrix least-squares methods using SHELXL-97. In the structure, the solvent molecules are highly disordered and cannot be modelled, thus the SQUEEZE routine of PLATON was applied to remove the contributions of the solvent molecules.[14] Crystal data and structure refinement parameters for the complexes are presented in Table S1 in the supporting information.

2.3 Synthesis of the organic ligands

5,5'-(benzo[c][1,2,5]furanzan-4,7-diyl) diisophthalate (H_4L1): To a mixture of 4,7-dibromobenzofuranzan (0.94 g, 3.40 mmol), dimethyl 5-(pinacolboryl)isophthalate (2.39 g, 7.46 mmol), Cs_2CO_3 (3.32 g, 10.18 mmol) and $Pd(PPh_3)_4$ (0.20 g, 0.17 mmol) were added dry dioxane (100 mL). The resulting mixture was stirred under reflux under a nitrogen atmosphere for 72 h. After removal of the solvents, CH_2Cl_2 (100 mL) and H_2O (100 mL) were added. The mixture was filtered through celite, and then washed with water and CH_2Cl_2. The organic phase was separated and the aqueous phase was extracted with CH_2Cl_2. The combined organic phase was washed with brine, dried over anhydrous $MgSO_4$ and concentrated by rato-evaporation. The residue was purified by recrystallization with toluene to give tetramethyl ester intermediate in 48% yield (0.82 g, 1.62 mmol). ^{1}H NMR ($CDCl_3$, 600 MHz) δ (ppm): 8.94 (d, J = 2.4 Hz, 4H), 8.82 (t, J = 2.4 Hz, 2H), 7.88 (s, 2H), 4.05 (s, 12H).

To tetramethyl ester intermediate (0.82 g, 1.62 mmol) in MeOH/THF (30/30 mL) was added 6 M NaOH aqueous solution (30 mL, 180 mmol). The resulting mixture was refluxed overnight. After removal of the solvents by rota-evaporation, the residue was dissolved in water and filtered. The filtrate was neutralized with conc. HCl in an ice-water bath. The precipitation was collected by filtration, washed with water and dried in vacuum at 343 K to give 5,5'-(benzo[c][1,2,5]furanzan-4,7-diyl) diisophthalate as a yellow solid in 99% yield (0.72 g, 1.60 mmol). ^{1}H NMR (DMSO-d_6, 600.1 MHz) δ (ppm): 13.33 (br, 4H), 8.87 (s, 4H), 8.57 (s, 2H), 8.17 (s, 2H); ^{13}C NMR (DMSO-d_6, 150.9 MHz) δ (ppm): 167.433, 149.257, 135.261, 134.357, 132.449, 131.049, 130.983, 127.261; Selected FTIR (KBr, cm^{-1}): 1707, 1603, 1458, 1421, 1375, 1279, 1217, 1169, 1039, 899, 860, 756, 715, 681, 665.

5,5'-(benzo[c][1,2,5]selenadiazole-4,7-diyl) diisophthalate (H_4L3): To a mixture of 4,7-dibromobenzo[c][1,2,5]selenadiazole (0.50 g, 1.47 mmol), dimethyl 5-(pinacolboryl)isophthalate (1.03 g, 3.23 mmol), Cs_2CO_3 (1.44 g, 4.40 mmol) and $Pd(PPh_3)_4$ (0.085 g, 0.07 mmol) were added dry dioxane (80 mL). The resulting mixture was stirred under reflux under a nitrogen atmosphere for 72 h. After the reaction mixture was cooled to room temperature and the organic solvent was removed under reduced pressure, CH_2Cl_2 (100 mL) and H_2O (100 mL) were then added. The mixture was filtered, washed with water and CH_2Cl_2. The organic phase was separated and the aqueous phase was

extracted with CH_2Cl_2. The combined organic phase was washed with brine, dried over anhydrous $MgSO_4$ and concentrated under reduced pressure to give crude product, which was purified by recrystallization with toluene to afford tetramethyl ester intermediate in 26.4% yield (0.22 g, 0.39 mmol). ^{1}H NMR ($CDCl_3$, 600 MHz) δ (ppm): 8.817-8.808 (m, 6H), 7.796 (s, 2H), 4.032 (s, 12H).

To tetramethyl ester intermediate (0.22 g, 0.39 mmol) in MeOH/THF (30/30 mL) was added 6 M NaOH aqueous solution (20 mL, 120 mmol). The resulting mixture was refluxed overnight. After removal of the solvents, the residue was dissolved in water and filtered. The filtrate was neutralized with conc. HCl in an ice-water bath. The precipitation was collected by filtration, washed with water and dried in vacuum at 343 K to give 5,5'-(benzo[c][1,2,5]selenadiazole-4,7-diyl) diisophthalate in 99% yield (0.72 g, 1.60 mmol). ^{1}H NMR (DMSO-d_6, 400.1 MHz) δ (ppm): 13.33 (br, 4H), 8.717 (s, 4H), 8.558 (s, 2H), 7.923 (s, 2H); ^{13}C NMR (DMSO-d_6, 100.6 MHz) δ (ppm): 167.070, 158.676, 138.800, 134.525, 133.415, 132.133, 129.928, 129.169; Selected FTIR (KBr, cm^{-1}): 1701, 1601, 1450, 1406, 1273, 1248, 1159, 1122, 918, 850, 758, 669.

2.4 Synthesis of the metal-organic frameworks

ZJNU-41: A mixture of $Cu(NO_3)_2{\cdot}3H_2O$ (15.0 mg, 62.1 μmol) and the organic ligand H_4L1 (5.0 mg, 11.1 μmol) was dissolved in a mixed solvent consisting of *N*,*N*'-dimethylformamide (DMF, 1.5 mL), methanol (0.5 mL) and water (0.08 mL) in a 20-mL glass vial. After the addition of 50 μL 6 M HCl, the vial was capped and heated at 353 K for 12 h. After cooling to room temperature, blue rhombus-shaped crystals were isolated by filtration in a yield 44% based on the organic ligand H_4L1. Selected FTIR (kBr, cm^{-1}): 1655, 1591, 1381, 1296, 1254, 1097, 1047, 877, 775, 758, 731, 661, 492; anal. for $C_{34}H_{44}Cu_2N_6O_{17}$, calcd: C, 43.64%, H, 4.74%, N, 8.98%; found: C, 43.59%, H, 4.80%, N, 8.75%.

ZJNU-42: A mixture of $CuCl_2{\cdot}2H_2O$ (15.0 mg, 88.0 μmol) and the organic linker H_4L3 (5.0 mg, 9.8 μmol) was dispersed in a mixed solvent consisting of DMF (1.5 mL), methanol (0.5 mL) and water (0.08 mL) in a 20-mL glass vial. After the addition of 80 μL 6 M HCl, the vial was capped and heated at 353 K for 36 h. Rhombus-shaped blue crystals were collected by filtration in a yield of 44% based on the organic ligand H_4L3. Selected FTIR (kBr, cm^{-1}): 1655, 1560, 1381, 1103, 1047, 775, 731; anal. for $C_{28}H_{26}Cu_2N_4O_{12}Se$, calcd: C, 41.18%, H, 3.21%, N, 6.86%; found: C, 41.22%, H, 3.15%, N, 6.79%.

2.5 Quantum chemical calculations

The van der Waals (vdW) corrected density functional theory (DFT) method, DFT-D2,[15] was employed to locate the occupation sites for CO_2 in **ZJNU-40**, **ZJNU-41**, and **ZJNU-42**. All of the calculations were performed in Vienna ab initio simulation package with version of vasp.5.3.3.[16] Periodic crystal structures were used in all of our calculations in order to include the confinement effect of the cavities in the materials capturing CO_2. The computational details for the CO_2 binding energy calculations were similar to our previous calculations of CO_2 adsorption in the three MOFs **ZJNU-43-45**.[17] Primitive cells for the three materials were employed to compute the CO_2 binding energies, and the lattice constants were fixed while all of the other atoms were fully relaxed. During the calculations all of the atoms were relaxed until the force on each ion was less than 0.01 eV Å^{-1}.

3. Results and discussion

3.1 Synthesis and characterization

The organic linkers H_4L1 and H_4L3 were synthesized by Suzuki cross-coupling reaction of dimethyl 5-(pinacolboryl) isophthalate and the corresponding dibromo compounds followed by hydrolysis and acidification. The detailed procedure was provided in experimental sections. The chemical structures of all the intermediates and target compounds were confirmed by NMR spectroscopy. Solvothermal reactions of Cu(II) salts and the organic linkers H_4L1 and H_4L3 under acidic conditions resulted in the formation of two Cu-based MOFs as highly crystalline products we termed **ZJNU-41** and **ZJNU-42**, respectively. Their structures were characterized by single-crystal X-ray diffraction. Powder X-ray diffraction studies showed that all peaks were in reasonably good agreement with the corresponding simulated patterns, confirming their phase purity (Fig. S1). Based on the single-crystal X-ray diffraction studies, TGA (Fig. S2), and elemental analyses, **ZJNU-41** and **ZJNU-42** can be best formulated as $[Cu_2L1(H_2O)_2]{\cdot}4DMF{\cdot}2H_2O$ and $[Cu_2L3(H_2O)_2]{\cdot}2DMF$, respectively.

3.2 Description of the crystal structures

Single-crystal X-ray diffraction analyses revealed that **ZJNU-41** and **ZJNU-42** adopted the same NbO-type network structure with **ZJNU-40**, crystallizing in *R*-3m space group. So the crystal structure of **ZJNU-41** was representatively described. Besides guest solvent molecules, the asymmetric unit of **ZJNU-41** contains one Cu^{2+} ions, one half of the deprotonated ligand, and one terminal water molecule. Each Cu centre is coordinated to four carboxylate oxygen atoms from four different ligands and one oxygen atom from the terminal water molecule in a square pyramidal geometry (Fig. 1a). Two adjacent Cu^{2+} ions were bridged by four carboxylate groups to form a dicopper paddlewheel SBU with a Cu-Cu separation of 2.653 Å, which is connected together by the organic linkers to form a three dimensional (3D) network (Fig. 1b). In the resulting framework, two different types of nanocages, shown in the Fig. 1c, can be observed with effective dimensions of *ca.* 14 Å and 14 × 25 Å, respectively, taking into account the van der Waals radius of the atoms. It is noteworthy that the cage surface is decorated with the highly polarized benzo[c][1,2,5]oxadiazole moieties whose local molecular dipole moment is perpendicular to the molecular long axis, thus providing additional binding sites for gas molecules. By comparison, it is clear that three MOFs have different functional sites polarizing the walls of nanocages (Fig. 1c-e). Analyses using PLATON software indicated the total solvent-accessible volumes after removal the guest and terminal water

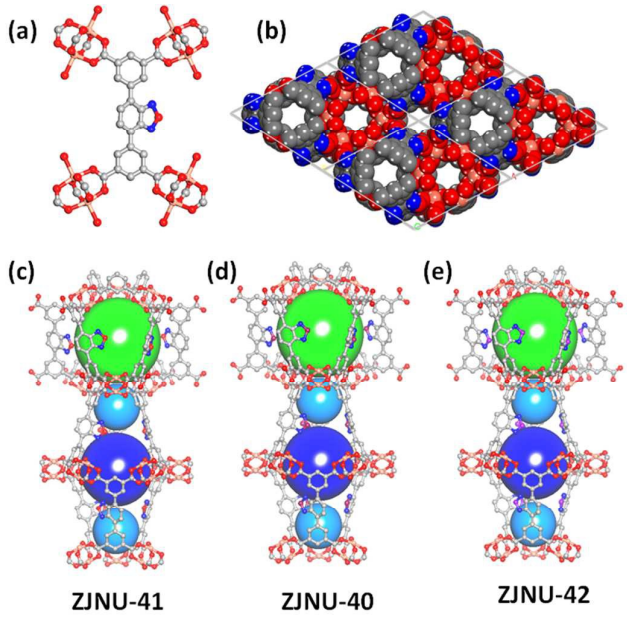

Fig. 1 Single-crystal X-ray structure of **ZJNU-41** showing the coordination environment of the organic linker $L1^{4-}$ (a), and 3D packing diagram along the *c* axis (b). Two different types of nanocages observed in **ZJNU-41** (c), **ZJNU-40** (d) and **ZJNU-42** (e).

molecules are approximately 61.7%, 59.5% and 57.9% for **ZJNU-41**, **ZJNU-40** and **ZJNU-42**, respectively, which is decreased in turn due to that the heteroatoms (O, S and Se) belonging to the heterocyclic rings attached to the organic linkers become heavier and heavier.

3.3 Permanent porosity

To establish the permanent porosity of these compounds, the N_2 adsorption isotherms were collected at 77 K using a Micrometric ASAP 2020 HD88 surface area and porosity analyser. Prior to measurements, the compounds were solvent-exchanged with dry acetone and evacuated under dynamic vacuum at room temperature followed by at 373 K until the degassed rate reached 3 μmHg min^{-1}. As shown in Fig. 2, the N_2 sorption isotherms revealed that all the three MOFs exhibit typical type-I adsorption behaviour, characteristic of microporous materials. At 77 K, the maximum amounts of N_2 taken up by **ZJNU-41a**, **ZJNU-40a** and **ZJNU-42a** (thereafter, "a" represents the activated form of MOF materials) were 645, 541, and 148 cm^3 (STP) g^{-1}, respectively. By applying the Brunauer–Emmett–Teller (BET) model, the apparent BET surface areas were estimated to be 2530, 2072, 572 m^2 g^{-1}, for **ZJNU-41a**, **ZJNU-40a** and **ZJNU-42a**, respectively (Fig. S3-5). The pore volumes determined from the maximum amount of N_2 adsorbed are 0.997, 0.837, 0.229 cm^3 g^{-1} for **ZJNU-41a**, **ZJNU-40a** and **ZJNU-42a**, respectively. We noted that both specific surface areas and pore volumes of the three MOF materials significantly decrease after grafting heterocyclic functional groups as compared to the parent MOF NOTT-101, which is understandable because the grafted functional groups occupied partial pore volume. For the three compounds, the decreasing trend of surface area can be also observed, which is

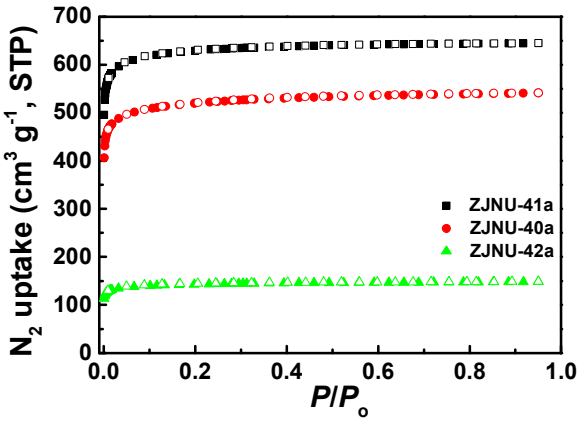

Fig. 2 N_2 sorption isotherms of **ZJNU-41a**, **ZJNU-40a** and **ZJNU-42a** at 77 K. Solid and open symbols represent adsorption and desorption, respectively. STP = standard temperature and pressure.

attributed to the fact that the incorporation of heavier heteroatoms into the ligands tends to increase the sample mass and occupy much more free void space within the porous structure. It is noteworthy that for **ZJNU-41a** and **ZJNU-40a**, the experimentally measured pore volumes are comparable to the theoretical values estimated by PLATON/VOID analysis, while for **ZJNU-42a**, the experimentally measured pore volume is significantly lower than the theoretical one of 0.707 cm^3 g^{-1}. These results indicate that after activation, **ZJNU-41a** and **ZJNU-40a** were desolvated completely and retained their structural integrity, while **ZJNU-42a** underwent partially collapse. Attempt to optimize activation temperatures to obtain the higher porosity of **ZJNU-42** failed.

3.4 CO_2 adsorption studies

The continuously increasing CO_2 level in the atmosphere has attracted worldwide attention during last a few decades due to its potential environmental damage. This motivates people to find various ways to capture CO_2 to mitigate the negative environmental effects CO_2 emission raised. Currently, the well-established strategy for CO_2 capture is chemical absorption by amine sorbents, which however suffers from some inherent drawbacks such as amine degradation, severe corrosion of equipment, and substantial energy consumptions. Due to the energy-efficient regeneration, adsorption-based separation was considered a promising alternative means. Therefore, the discovery and development of high performance adsorbents to capture CO_2 is paramount. Among various porous materials explored, MOFs have shown huge potentials in this regards due to their favourable structure features such as tuneable pore size and modifiable pore surface.[18]

Successful incorporation of different heterocyclic moieties into the isostructural frameworks provides a platform for investigating how these heterocyclic functional sites have an effect on the CO_2 adsorption and therefore prompted us to study their CO_2 adsorption properties. Accordingly, CO_2 sorption isotherms were measured systematically at three different temperatures of 278 K, 288 K and 298 K and the

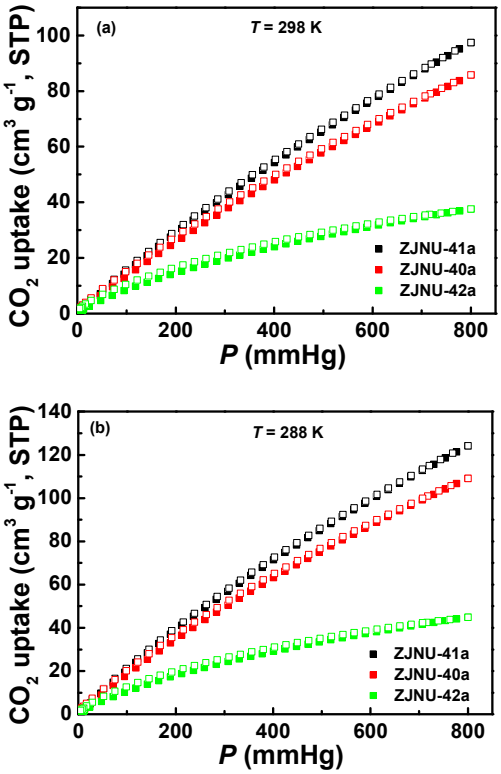

Fig. 3 CO_2 adsorption-desorption isotherms of **ZJNU-41**, **ZJNU-40a** and **ZJNU-42a** at 298 K (a) and 288 K (b). Solid and open symbols represent adsorption and desorption, respectively.

Table 1 CO_2 adsorption in Cu-based NbO-type MOFs

MOFs	CO_2 uptake at 1 atm [cm^3 (STP) g^{-1}]	V_p (cm^3 g^{-1})	BET (m^2 g^{-1})	*Ref.*
QI-Cu	102[a]	0.662	1631	19
NJU-Bai14	100[b]	0.924	2384	8c
ZJNU-41	97.4[b]	0.997	2530	This work
HNUST-1	93[b]	0.571	1400	9
NOTT-125	92.59[b]	1.1	2447	20
HNUST-3	85[b]	0.99	2412	21
NOTT-101	83[c]	1.080	2805	10
SNU-50	80[b]	1.08	2300	8h
NU-135	80[b]	1.02	2600	8e
MOF-505	73[b]	NA	NA	22
UTSA-40	73[c]	0.65	1630	23
NOTT-102	72[c]	1.268	3342	10

[a] 293 K; [b] 298 K; [c] 296 K;

pressure up to 1 bar. As shown in Fig. 3, all isotherms show excellent reversibility without any hysteresis, indicating that vacuum can remove all CO_2 molecules during the desorption process. The CO_2 adsorption capacities at 298 K and 1 atm reach 97.4, 85.7, and 37.6 cm^3 (STP) g^{-1}, for **ZJNU-41a**, **ZJNU-40a**, and **ZJNU-42a**, respectively, which is increased to 124.2,

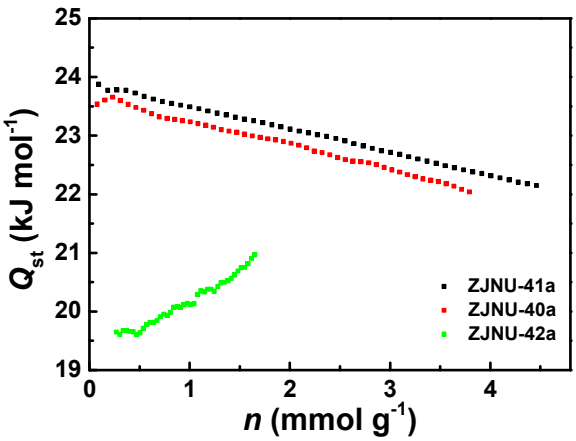

Fig. 4 The isosteric heat of CO_2 adsorption for **ZJNU-41a**, **ZJNU-40a** and **ZJNU-42a** as a function of CO_2 loading.

109.1, and 44.9 cm^3 (STP) g^{-1}, respectively, when the temperature is lowered to 288 K. Notably, the CO_2 uptakes follow the hierarchy of **ZJNU-41a** > **ZJNU-40a** > **ZJNU-42a**. A comparison with the related NbO-type MOFs is presented in Table 1. It can be seen that the CO_2 capacity of **ZJNU-41a** is comparable and even superior to those reported in NbO-type frameworks, such as NJU-bai14 (100 cm^3 (STP) g^{-1})[8c], NOTT-125 (93 cm^3 (STP) g^{-1})[20], HNUST-1 (93 cm^3 (STP) g^{-1})[9], NOTT-101 (83 cm^3 (STP) g^{-1})[10], SNU-50 (80 cm^3 (STP) g^{-1}),[8h] NU-135 (79 cm^3 (STP) g^{-1}),[8e] MOF-505 (73 cm^3 (STP) g^{-1}),[22] NOTT-102 (72 cm^3 (STP) g^{-1})[10].

To better understand the role of these heterocyclic rings, we analysed the interactions between CO_2 and frameworks by calculating the isosteric heats (Q_{st}) of CO_2 adsorption using Clausius-Claperyron equation on the basis of the adsorption isotherms collected at 278, 288 and 298 K. From Fig. 4, it can be observed that as CO_2 loading increases, Q_{st} of CO_2 adsorption for **ZJNU-40a** and **ZJNU-41a** decreases, while that for **ZJNU-42a** initially keeps almost constant before 0.5 mmol g^{-1} of CO_2 loadings, and then begins to increase. The latter might be due to attractive CO_2-CO_2 interactions, which become important at higher loadings, especially in metal-organic frameworks with small pore. The Q_{st} values for the three MOFs were in the range of 19-24 kJ mol^{-1}, which is moderate compared to those reported in metal-organic frameworks with high density of open metal sites.[24] More importantly, **ZJNU-41a** possessed the higher Q_{st} values through the adsorption process compared to **ZJNU-40a** and **ZJNU-42a**, suggesting that a stronger interaction between CO_2 molecules and **ZJNU-41a**, which is unexpected because the increasing basicity (or pK_a value) of nitrogen sites in heterocyclic rings in the order of benzo[c][1,2,5]oxadiazole < benzo[c][1,2,5]thiadiazole < benzo[c][1,2,5]selenadiazole, combined with the increase of the overlapping potentials for CO_2 adsorption due to the decrease in the pore size, should lead to the stronger affinity of pore surface towards CO_2 molecules. To figure out the underlying reason why **ZJNU-41a** has higher adsorption heat, we calculated using Chemical 3D

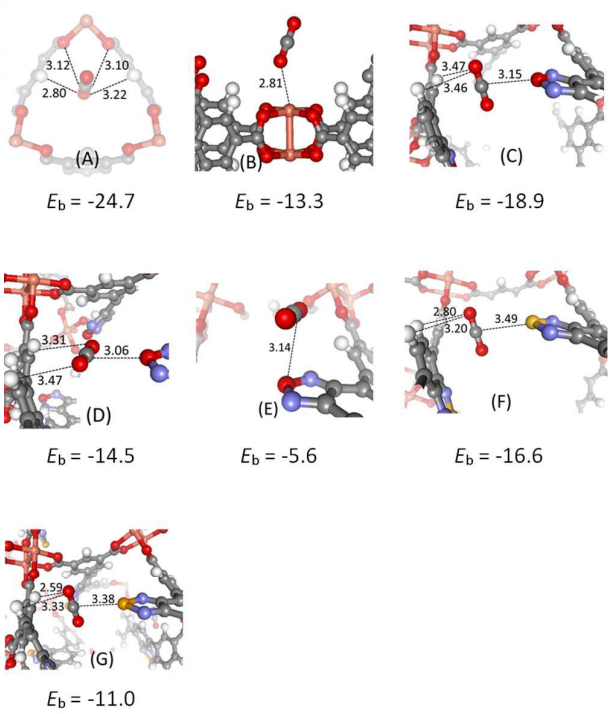

Fig. 5 Five optimized structures (A-E) representing the typical adsorption sites for CO_2 in **ZJNU-41** are shown, as well as hydrogen bond lengths and the DFT-D2 calculated binding energies. Structures F and G are the most favorable adsorption sites surrounding the organic linkers in **ZJNU-40** and **ZJNU-42**, respectively. The units for bond distance and binding energy are Å and kJ mol^{-1}. The O, H, C, Cu, N, S, and Se atoms are represented with red, white, grey, brown, yellow, and orange balls, respectively.

software the molecular dipole of these heterocyclic moieties attached to the organic linkers. The molecule dipoles are 4.20, 3.17, and 0.09 Debye for benzo[c][1,2,5]oxadiazole, benzo[c][1,2,5]thiadiazole, and benzo[c][1,2,5]selenadiazole, respectively. Therefore, considering that the three MOFs are isostructural, and low-pressure CO_2 uptake capacity is strongly correlated with the CO_2 affinity towards the framework, we speculate that the higher molecular dipole of benzo[c][1,2,5]oxadiazole incorporated to the framework of **ZJNU-41a** might be primarily responsible for the stronger dipole-quadrupole interactions between CO_2 and **ZJNU-41a**, thus explaining the higher CO_2 uptake capacity of **ZJNU-41a**. This also demonstrates that incorporation of highly polarized heterocyclic moieties will favourably enhance CO_2 adsorption.

3.5 Quantum Chemical Calculations

The three MOFs have almost the same crystal structures except the organic linkers, where the O atom in H_4L1 organic linker (**ZJNU-41**) was replaced by S and Se in H_4L2 (**ZJNU-40**) and H_4L3 (**ZJNU-42**), respectively. Thus it is reasonable to expect that the CO_2 adsorption mechanism in the three materials is very similar except the adsorption sites around the organic linkers, since the dipole moments for the three linkers (see Scheme 1) are different, i.e., 6.23, 4.80, and 2.61 Debye for H_4L1, H_4L2, and H_4L3, respectively. Many different initial configurations have been considered for each material and several typical structures were obtained as shown in Fig. 5. The binding energy was calculated as:

$$E_b = E_{gas/MOF} - E_{gas} - E_{MOF}$$

where $E_{gas/MOF}$, E_{gas}, and E_{MOF} represent the energies for CO_2 adsorbed **ZJNU-40 (41, 42)**, isolated CO_2 molecule, and pure **ZJNU-40 (41, 42)** material, respectively. Take **ZJNU-41** for example, the most favourable occupation site is the triangular window site (see structure A in Fig. 5) with E_b of -24.7 kJ mol^{-1}, very similar to -25.1 to -26.1 kJ mol^{-1} at the same adsorption site for the three MOFs **ZJNU-43-45** we reported recently.[17] The CO_2 binding energy at the open metal site (structure B) is -13.3 kJ mol^{-1}, only slightly larger than -11.8 to -12.8 kJ mol^{-1} at the same adsorption sites in **ZJNU-43-45**. This is expected since the chemical environment for the CO_2 adsorption are almost the same at the triangular window sites and open metal sites between **ZJNU-41** and **ZJNU-43-45**. However, the organic linkers for the MOFs we studied are different, and thus the binding energies for CO_2 surrounding the organic linkers should also be different. Indeed, our calculations indicate that the structure C has the strongest adsorption affinity E_b = -18.9 kJ mol^{-1} surrounding the organic linker H_4L1, which is much smaller than -27.6 kJ mol^{-1} in **ZJNU-44** with the best accessible N atoms[17] and is close to -18.1 and -18.7 kJ mol-1 in **ZJNU-43** and **ZJNU-45** with less accessible N atoms. We also found the structure C has a perpendicular orientation for CO_2 with respect to the organic ring, of which the adsorption affinity is stronger than those with different orientation, i.e., -14.5 and -5.6 kJ mol^{-1} for structures D (on the plane of organic ring) and E (on the top of organic ring). Furthermore, our calculations indicate that the adsorption affinities for CO_2 in **ZJNU-40** and **ZJNU-42** are similar to those in **ZJNU-41** except the adsorption sites at the organic linkers. The structures F and G (Fig. 5) represent the most favorable adsorption sites surrounding the organic linkers in **ZJNU-40** and **ZJNU-42**, respectively, with the binding energies of -16.6 and -11.0 kJ mol^{-1}, smaller than -18.9 kJ mol^{-1} for structure C in **ZJNU-41**. This agrees well with the order of the magnitude of dipole moments for the organic linkers H_4L1 (**ZJNU-41**), H_4L2 (**ZJNU-40**), and H_4L3 (**ZJNU-42**). Summarizing, our vdW corrected DFT-D2 methods based calculations confirm that the organic linkers in the three materials **ZJNU-40-42** have different adsorption affinity for CO_2, thus well explaining their different CO_2 adsorption capacities.

4. Conclusions

We designed and synthesized three new organic ligands by grafting highly polarized functional groups to terphenyl-3,3''-,5,5''-tetracarboxylic acid, and used them to construct three MOFs, which were characterized by single-crystal X-ray diffraction studies to have the same structure of NbO-type. By introduction of these heterocyclic ring units with different polarizabilities, the CO_2 uptakes can be systematically tailored. Furthermore, **ZJNU-41a** exhibited much higher adsorption capacity for CO_2 compared with the other two MOFs materials **ZJNU-40a** and **ZJNU-42a**. Such high CO_2 uptake capacity of

ZJNU-41a is believed to be primarily due to incorporation of the higher molecular dipole of benzo[c][1,2,5]oxadiazole into the frameworks, relative to benzo[c][1,2,5]thiadiazole and benzo[c][1,2,5]selenadiazole, which leads to stronger dipole-quadrupole interaction between CO_2 and **ZJNU-41a**. This work demonstrates that introduction of highly polarized heterocyclic rings into the framework affords a promising method for the development of metal-organic framework materials with better CO_2 adsorption capacity.

Acknowledgments

This work was supported by the National Natural Science Foundation of China (No. 21301156), Open Research Fund of Top Key Discipline of Chemistry in Zhejiang Provincial Colleges and Key Laboratory of the Ministry of Education for Advanced Catalysis Materials (ZJHX201313), and Qianjiang talents project in Zhejiang province (ZC304015017). D.-L. Chen gratefully acknowledges the financial support from the National Natural Science Foundation of China (21303165).

Notes and references

1 O. M. Yaghi, G. Li and H. Li, *Nature*, 1995, **378**, 703-706.
2 S. Kitagawa, R. Kitaura and S.-i. Noro, *Angew. Chem. Int. Ed.*, 2004, **43**, 2334-2375.
3 (a) Y. He, W. Zhou, G. Qian and B. Chen, *Chem. Soc. Rev.*, 2014, **43**, 5657-5678; (b) M. P. Suh, H. J. Park, T. K. Prasad and D.-W. Lim, *Chem. Rev.*, 2012, **112**, 782-835; (c) R. B. Getman, Y.-S. Bae, C. E. Wilmer and R. Q. Snurr, *Chem. Rev.*, 2012, **112**, 703-723; (d) K. Sumida, D. L. Rogow, J. A. Mason, T. M. McDonald, E. D. Bloch, Z. R. Herm, T.-H. Bae and J. R. Long, *Chem. Rev.*, 2012, **112**, 724-781; (e) H. Wu, Q. Gong, D. H. Olson and J. Li, *Chem. Rev.*, 2012, **112**, 836-868; (f) J.-R. Li, J. Sculley and H.-C. Zhou, *Chem. Rev.*, 2012, **112**, 869-932; (g) Y. He, W. Zhou, R. Krishna and B. Chen, *Chem. Commun.*, 2012, **48**, 11813-11831.
4 (a) L. Ma, C. Abney and W. Lin, *Chem. Soc. Rev.*, 2009, **38**, 1248-1256; (b) J. Lee, O. K. Farha, J. Roberts, K. A. Scheidt, S. T. Nguyen and J. T. Hupp, *Chem. Soc. Rev.*, 2009, **38**, 1450-1459; (c) A. Corma, H. García and F. X. L. i. Xamena, *Chem. Rev.*, 2010, **110**, 4606-4655; (d) M. Yoon, R. Srirambalaji and K. Kim, *Chem. Rev.*, 2012, **112**, 1196-1231; (e) G. Nickerl, A. Henschel, R. Grünker, K. Gedrich and S. Kaskel, *Chem. Ing. Tech.*, 2011, **83**, 90-103.
5 (a) Y. Cui, Y. Yue, G. Qian and B. Chen, *Chem. Rev.*, 2012, **112**, 1126-1162; (b) L. E. Kreno, K. Leong, O. K. Farha, M. Allendorf, R. P. V. Duyne and J. T. Hupp, *Chem. Rev.*, 2012, **112**, 1105-1125.
6 P. Horcajada, R. Gref, T. Baati, P. K. Allan, G. Maurin, P. Couvreur, G. Férey, R. E. Morris and C. Serre, *Chem. Rev.*, 2012, **112**, 1232-1268.
7 Y. He, B. Li, M. O'Keeffe and B. Chen, *Chem. Soc. Rev.*, 2014, **43**, 5618-5656.
8 (a) B. Li, H.-M. Wen, H. Wang, H. Wu, T. Yildirim, W. Zhou and B. Chen, *Energy Environ. Sci.*, 2015, **8**, 2504-2511; (b) Y. Yan, S. Yang, A. J. Blake and M. Schröder, *Acc. Chem. Res.*, 2014, **47**, 296-307; (c) M. Zhang, Q. Wang, Z. Lu, H. Liu, W. Liu and J. Bai, *CrystEngComm*, 2014, **16**, 6287-6290; (d) X. Rao, J. Cai, J. Yu, Y. He, C. Wu, W. Zhou, T. Yildirim, B. Chen and G. Qian, *Chem. Commun.*, 2013, **49**, 6719-6721; (e) R. D. Kennedy, V. Krungleviciute, D. J. Clingerman, J. E. Mondloch, Y. Peng, C. E. Wilmer, A. A. Sarjeant, R. Q. Snurr, J. T. Hupp, T. Yildirim, O. K. Farha and C. A. Mirkin, *Chem. Mater.*, 2013, **25**, 3539-3543; (f) D. Zhao, D. Yuan, A. Yakovenko and H.-C. Zhou, *Chem. Commun.*, 2010, **46**, 4196-4198; (g) D. Sun, S. Ma, J. M. Simmons, J.-R. Li, D. Yuan and H.-C. Zhou, *Chem. Commun.*, 2010, **46**, 1329-1331; (h) T. K. Prasad, D. H. Hong and M. P. Suh, *Chem. Eur. J.*, 2010, **16**, 14043-14050; (i) X. Lin, I. Telepeni, A. J. Blake, A. Dailly, C. M. Brown, J. M. Simmons, M. Zoppi, G. S. Walker, K. M. Thomas, T. J. Mays, P. Hubberstey, N. R. Champness and M. Schröder, *J. Am. Chem. Soc.*, 2009, **131**, 2159-2171; (j) X. Lin, J. Jia, X. Zhao, K. M. Thomas, A. J. Blake, G. S. Walker, N. R. Champness, P. Hubberstey and M. Schröder, *Angew. Chem. Int. Ed.*, 2006, **45**, 7358-7364.
9 B. Zheng, H. Liu, Z. Wang, X. Yu, P. Yia and J. Bai, *CrystEngComm*, 2013, **15**, 3517-3520.
10 C. Song, Y. He, B. Li, Y. Ling, H. Wang, Y. Feng, R. Krishna and B. Chen, *Chem. Commun.*, 2014, **50**, 12105-12108.
11 N. Blouin, A. Michaud, D. Gendron, S. Wakim, E. Blair, R. Neagu-Plesu, M. Belletête, G. Durocher, Y. Tao and M. Leclerc, *J. Am. Chem. Soc.*, 2008, **130**, 732-742.
12 R. Yang, R. Tian, Q. Hou, W. Yang and Y. Cao, *Macromolecules*, 2003, **36**, 7453-7460.
13 G. M. Sheldrick, Acta Crystallogr. Sect. A, 2008, 64, 112.
14 A. L. Spek, J. Appl. Crystallogr., 2003, 36, 7.
15 S. Grimme, *J. Comput. Chem.*, 2006, **27**, 1787-1799.
16 (a) G. Kresse, *J. Non-Cryst. Solid*, 1995, **193**, 222-229; (b) G. Kresse and J. Hafner, *Phys. Rev. B*, 1994, **49**, 14251-14264; (c) G. Kresse and J. Furthmüller, *Phys. Rev. B*, 1996, **54**, 11169-11186; (d) G. Kresse and J. Furthmüller, *Comput. Mater. Sci.*, 1996, **6**, 15-50.
17 C. Song, J. Hu, Y. Ling, Y. Feng, R. Krishna, D.-l. Chen and Y. He, *J. Mater. Chem. A*, 2015, **3**, 19417-19426.
18 (a) S.-J. Bao, R. Krishna, Y.-B. He, J.-S. Qin, Z.-M. Su, S.-L. Li, W. Xie, D.-Y. Du, W.-W. He, S.-R. Zhang and Y.-Q. Lan, *J. Mater. Chem. A*, 2015, **3**, 7361-7367; (b) R. Luebke, Ł. J. Weseliński, Y. Belmabkhout, Z. Chen, Ł. Wojtas and M. Eddaoudi, *Cryst. Growth Des.*, 2014, **14**, 414-418 ; (c) S. Biswas, J. Zhang, Z. Li, Y.-Y. Liu, M. Grzywa, L. Sun, D. Volkmer and P. V. D. Voort, *Dalton Trans.*, 2013, **42**, 4730-4737; (d) L. Du, Z. Lu, K. Zheng, J. Wang, X. Zheng, Y. Pan, X. You and J. Bai, *J. Am. Chem. Soc.*, 2013, 562-565; (e) E. Yang, H.-Y. Li, F. Wang, H. Yang and J. Zhang, *CrystEngComm*, 2013, **15**, 658-661; (f) T. Panda, K. M. Gupta, J. Jiang and R. Banerjee, *CrystEngComm*, 2014, **16**, 4677-4680; (g) H.-L. Jiang, D. Feng, T.-F. Liu, J.-R. Li and H.-C. Zhou, *J. Am. Chem. Soc.*, 2012, **134**, 14690-14693; (h) J. Qian, F. Jiang, D. Yuan, M. Wu, S. Zhang, L. Zhang and M. Hong, *Chem. Commun.*, 2012, **48**, 9696-9698; (i) B. Li, Z. Zhang, Y. Li, K. Yao, Y. Zhu, Z. Deng, F. Yang, X. Zhou, G. Li, H. Wu, N. Nijem, Y. J. Chabal, Z. Lai, Y. Han, Z. Shi, S. Feng and J. Li, *Angew. Chem. Int. Ed.*, 2012, **51**, 1412-1415; (j) W.-Y. Gao, W. Yan, R. Cai, K. Williams, A. Salas, L. Wojtas, X. Shi and S. Ma, *Chem. Commun.*, 2012, **48**, 8898-8900; (k) Y. Ling, F. Yang, M. Deng, Z. Chen, X. Liu, L. Weng and Y. Zhou, *Dalton Trans.*, 2012, **41**, 4007-4011; (l) M.-S. Chen, M. Chen, S. Takamizawa, T.-a. Okamura, J. Fan and W.-Y. Sun, *Chem. Commun.*, 2011, **47**, 3787-3789; (m) Q. Lin, T. Wu, S.-T. Zheng, X. Bu and P. Feng, *J. Am. Chem. Soc.*, 2012, **134**, 784-787; (n) R. Vaidhyanathan, S. S. Iremonger, G. K. H. Shimizu, P. G. Boyd, S. Alavi and T. K. Woo, *Science*, 2010, **330**, 650-653; (o) A. Demessence, D. M. D'Alessandro, M. L. Foo and J. R. Long*, *J. Am. Chem. Soc.*, 2009, **131**, 8784-8786.
19 C. Wang, L. Li, S.-F. Tang and X. Zhao, *ACS Appl. Mater. Interfaces*, 2014, **6**, 16932-16940.
20 N. H. Alsmail, M. Suyetin, Y. Yan, R. Cabot, C. P. Krap, J. Lü, T. L. Easun, E. Bichoutskaia, W. Lewis, A. J. Blake and M. Schröder, *Chem. Eur. J.*, 2014, **20**, 7317-7324.

21 Z. Wang, B. Zheng, H. Liu, X. Lin, X. Yu, P. Yi and R. Yun, *Cryst. Growth Des.*, 2013, **13**, 5001-5006.
22 A. R. Millward and O. M. Yaghi, *J. Am. Chem. Soc.*, 2005, **127**, 17998-17999.
23 Y. He, S. Xiang, Z. Zhang, S. Xiong, C. Wu, W. Zhou, T. Yildirim, R. Krishna and B. Chen, *J. Mater. Chem. A*, 2013, **1**, 2543-2551.
24 (a) S. R. Caskey, A. G. Wong-Foy and A. J. Matzger, *J. Am. Chem. Soc.*, 2008, **130**, 10870-10871; (b) P. L. Llewellyn, S. Bourrelly, C. Serre, A. Vimont, M. Daturi, L. Hamon, G. D. Weireld, J.-S. Chang, D.-Y. Hong, Y. K. Hwang, S. H. Jhung and G. Férey, *Langmuir*, 2008, **24**, 7245-7250.

TOC

By introduction of different heterocyclic moieties with varied polarizability into isostructural metal-organic frameworks, the CO_2 uptakes can be systematically tailored.